Monthly Notices of the ROYAL ASTRONOMICAL SOCIETY

MNRAS **471,** 1045–1055 (2017) doi:10.1093/mnras/stx1631
Advance Access publication 2017 June 29

High-redshift radio galaxies and divergence from the CMB dipole

Jacques Colin,[1,2] Roya Mohayaee,[1,2★] Mohamed Rameez[2★] and Subir Sarkar[2,3★]

[1]*Sorbonne Universités, UPMC Univ Paris 06, CNRS, Institut d'Astrophysique de Paris, F-98 bis Bld Arago, Paris F-75014, France*
[2]*Niels Bohr Institute, University of Copenhagen, Blegdamsvej 17, DK-2100 Copenhagen Ø, Denmark*
[3]*Rudolf Peierls Centre for Theoretical Physics, University of Oxford, 1 Keble Road, Oxford OX1 3NP, UK*

Accepted 2017 June 26. Received 2017 May 23; in original form 2017 March 26

ABSTRACT

Previous studies have found our velocity in the rest frame of radio galaxies at high redshift to be much larger than that inferred from the dipole anisotropy of the cosmic microwave background. We construct a full sky catalogue, NVSUMSS, by merging the NRAO VLA Sky Survey and the Sydney University Molonglo Sky Survey catalogues and removing local sources by various means including cross-correlating with the 2MASS Redshift Survey catalogue. We take into account both aberration and Doppler boost to deduce our velocity from the hemispheric number count asymmetry, as well as via a three-dimensional linear estimator. Both its magnitude and direction depend on cuts made to the catalogue, e.g. on the lowest source flux; however these effects are small. From the hemispheric number count asymmetry we obtain a velocity of 1729 ± 187 km s^{-1}, i.e. about four times *larger* than that obtained from the cosmic microwave background dipole, but close in direction, towards RA=$149^{\circ} \pm 2^{\circ}$, Dec. = $-17^{\circ} \pm 12^{\circ}$. With the three-dimensional estimator, the derived velocity is 1355 ± 174 km s^{-1} towards RA = $141^{\circ} \pm 11^{\circ}$, Dec. = $-9^{\circ} \pm 10^{\circ}$. We assess the statistical significance of these results by comparison with catalogues of random distributions, finding it to be 2.81σ (99.75 per cent confidence).

Key words: catalogues – large-scale structure of Universe – cosmology: observations – cosmology: theory.

1 INTRODUCTION

The cosmic microwave background (CMB) exhibits a dipole anisotropy (Bracewell & Conklin 1968; Henry 1971; Smoot, Gorenstein & Muller 1977) which is 1000 times bigger than the primordial temperature fluctuations first detected by *COBE* (Kogut et al. 1993). An observer moving through an isotropic radiation field would observe such a dipole (Stewart & Sciama 1967; Peebles & Wilkinson 1968) and conversely the observed dipole can be used to infer the velocity of the observer. Indeed the velocity of the Solar system (and our Local Group) is inferred from the CMB temperature dipole assuming that the latter is entirely due to our motion.

Although a kinematic origin is the most plausible interpretation of the CMB dipole, one can consider other mechanisms which may be, at least partially, responsible (Paczynski & Piran 1990; Langlois & Piran 1996). An independent measurement of our velocity is therefore desirable. It has been suggested that this can be done by measuring the aberration of the CMB (Challinor & van Leeuwen 2002; Burles & Rappaport 2006); however the effect is too small to be detected with $>3\sigma$ significance even using the best available data to date (Planck Collaboration XXVII 2014).

If the dipole is due to our motion then it requires the Universe to be anisotropic at least locally. Indeed, galaxy surveys do exhibit such an anisotropy. Along the direction of the CMB dipole lie the most massive neighbouring superclusters: Virgo, the Great Attractor Hydra-Centaurus, Coma, Hercules and Shapley, and possibly yet-to-be-mapped superclusters beyond these (see Table 1). The gravitational attraction of these structures is evidently pulling us in the direction indicated by the CMB dipole. However detailed maps of the local Universe, e.g. from the infrared 2MASS Redshift Survey (2MRS) or supernova catalogues, show that the full dipole *cannot* be attributed to these structures and at least 20 per cent remains unaccounted for (Lauer & Postman 1994; Hudson et al. 2004; Watkins, Feldman & Hudson 2009; Lavaux et al. 2010; Feldman, Watkins & Hudson 2010; Colin et al. 2011; Magoulas et al. 2012; Feindt et al. 2013; Watkins & Feldman 2015). It is thus necessary to go beyond even Shapley (at ∼262 Mpc) to establish if there is indeed convergence to the CMB frame at larger scales – as is essential if the universe is to be described as homogeneous when averaged on such scales.

However, there are no full-sky optical galaxy redshift surveys extending well beyond Shapley and previous studies in this context have therefore suffered from lack of full sky coverage (e.g.

★ E-mail: mohayaee@iap.fr (RM); mohamed.rameez@nbi.ku.dk (MR); subir.sarkar@physics.ox.ac.uk (SS)

Table 1. Local superclusters which are responsible for a large part of the CMB dipole (Lavaux et al. 2010; Colin et al. 2011).

Name	{RA°, Dec.°}
Virgo	{186.8, 12}
Hydra & Centaurus (Great Attractor)	{192.2, −38}
Norma	{243, −59}
Persus-Pisces	{27.5, 36}
Coma	{195.0, 28.0}
Hercules	{241.3, 17.8}
Shapley	{201.3, −30}
Ophiuchus	{255, −8}

Plionis, Coles & Catelan 1993; Itoh, Yahata & Takada 2010). Further complications arise when using other catalogues such as of galaxy clusters to search for the expected dipole signal (e.g. Chluba, Hütsi & Sunyaev 2005). There have in fact been persistent reports of an anomalous 'dark flow' on large scales traced by the kinematic Sunyaev–Zel'dovich effect in clusters, in roughly the same direction as the CMB dipole (Kashlinsky, Atrio-Barandela & Kocevski 2008; Atrio-Barandela et al. 2015).

On the other hand, radio galaxies are extremely luminous, can be observed up to high redshifts, and are unaffected by dust obscuration. However early analyses of the dipole in the distribution of radio galaxies suffered from the severe sparseness of their catalogues (Baleisis et al. 1998). Hence, such studies have become feasible only after the NRAO VLA Sky Survey (NVSS). This is a catalogue of nearly two million radio galaxies covering the sky above declination of −40°. NVSS has been used extensively to search for convergence to the CMB dipole and most previous studies have found an interesting *discrepancy* with the CMB measurement of our local velocity (Singal 2011; Gibelyou & Huterer 2012; Rubart & Schwarz 2013; Tiwari et al. 2015; Tiwari & Jain 2015).

While the velocity of the Solar system barycentre inferred from the CMB temperature dipole anisotropy is 369 km s^{-1}, the value inferred from NVSS ranges from 700 km s^{-1} (Blake & Wall 2002) to over 2000 km s^{-1} (Gibelyou & Huterer 2012). We too find a similarly large velocity and demonstrate that it depends only mildly on the characteristics of the data sets used: e.g. the width of the Galactic and super-Galactic plane strips removed from the survey and the lower and upper limits on the flux. Significantly, the direction of the velocity is quite robust and well aligned with the direction of the CMB dipole.

It is hard to understand how such a large difference can have a physical explanation. Previous works (Paczynski & Piran 1990; Langlois & Piran 1996; Ghosh 2014) have invoked horizon-scale isocurvature perturbations as an alternative to the kinematic origin for the CMB dipole. Here, however, we are observing a dipole far *larger* than that inferred from CMB itself, but still at high redshift. In addition local data – specifically distance and redshift catalogues – indicate that at low redshifts a good part of the CMB dipole is recovered by ∼250 Mpc. Although the present data do not allow us to fully explore how the convergence to CMB develops as we go deeper into the Universe and in redshift space, the radio data at redshift $z \sim 1$ clearly indicate that a significantly *larger* dipole exists in the rest frame of the radio galaxies. The origin of this difference from the CMB dipole is a real mystery and deserves closer examination.

A possible explanation is systematics due to the incomplete sky coverage of NVSS which can generate a spurious dipole (Gibelyou & Huterer 2012; Tiwari & Nusser 2016). Various methods have been used to restore the symmetry required for a robust dipole analysis such as cutting out the NVSS catalogue above declination of 40° (Singal 2011) or removing the Galactic and counter-Galactic plane (Rubart & Schwarz 2013). Our work elaborates on previous studies in several ways. We construct a *full-sky* catalogue, which we call NVSUMSS, by patching the NVSS with its southern-sky counterpart – the Sydney University Molonglo Sky Survey (SUMSS). This results in a catalogue with about 600 000 radio sources with flux above 10 mJy after cutting out a strip of ±10° around the Galactic plane in NVSS to match the corresponding cut in SUMSS.

Another possible systematic which has often been discussed is contamination by local sources. It is well known that a large part of the CMB dipole anisotropy is due to the anisotropic local distribution of matter (Lavaux et al. 2010; Colin et al. 2011). Past studies have tried to clean NVSS from such local source contamination either by removing individual large local structures (Blake & Wall 2002) or by cutting out the super-Galactic plane in which the majority of local superclusters lie (Tiwari et al. 2015). However, even after all these cuts the radio dipole extracted by all previous studies remains well above that inferred from the CMB. To fully eliminate the contribution from the local structures, we adopt several strategies. First we cross-correlate NVSUMSS with the catalogue (van Velzen et al. 2012) of local radio sources (LRS) and remove patches (of increasing area) around these sources from NVSUMSS catalogue. Our results are not, however, significantly altered by doing so. As the LRS catalogue is limited to sources brighter than 200 mJy, we go further by next removing eight dominant local superclusters from Virgo to Ophiuchus. Previous studies have shown that these local structures are responsible for nearly 80 per cent of the CMB dipole. Even so their removal does not alter our results significantly. We then remove the super-Galactic plane completely by cutting out a ±10° strip around it. This too has little effect. Finally we cross-correlate NVSUMSS with the 2MRS catalogue, and remove zones of increasingly larger areas around the 2MRS sources from the NVSUMSS catalogue. This too has no significant impact.

Because of evolution, the fraction of nearby radio sources is low even at large flux densities, the median redshift of radio sources in complete samples with flux ranging from mJy to Jy being $z \sim 0.8$ (Condon 1989). The fact that the redshift distribution of complete samples of radio sources peaks at $z \sim 1$ for flux-densities down to ∼10 mJy implies that local sources are swamped by more numerous distant ones (de Zotti et al. 2010). The mean redshift of NVSS sources is estimated to be above 1 (Ho et al. 2008; de Zotti et al. 2010). Thus most of the sources in our NVSUMSS catalogue lie at high redshift and by removing local sources through cross-correlation of NVSUMSS with the 2MRS catalogue we ensure that they constitute a uniform background. Our motion with respect to such a uniform background causes the aberration of light and the sources would thus be displaced in the sky by an angle that depends on our velocity. More sources would be observed in the direction of the motion than in the opposite direction.

Thus, by measuring the aberration angle, we infer the velocity of the Solar system (or the Local Group) barycentre in the rest frame of the distant radio galaxies. A catalogue with good sky coverage would exhibit a hemispherical asymmetry which peaks when the plane of hemisphere is perpendicular to the direction of the motion. A simple formula can be used to determine the aberration angle and hence our velocity in the rest frame of the radio sources. Aberration analysis is very powerful in the sense that it is *independent*

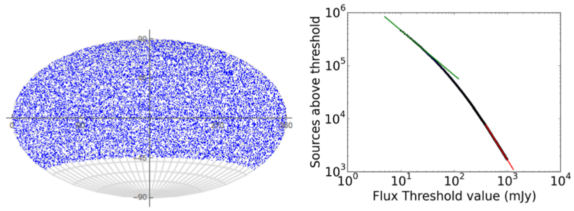

Figure 1. The left panel is the Aitoff projection in equatorial coordinates (RA and Dec.) of the full NVSS catalogue. The right panel shows how the integral number count changes with the flux threshold.

of distance and so can be used in conjunction with a full-sky photometric galaxy survey, as long as there are no observational biases generating spurious anisotropies. In fact, the motion of the observer also results in Doppler boosting of the frequency at which the sources are observed – as a result more sources will be observed in the direction of the motion. Unlike aberration, Doppler boosting depends on the flux and it is known that for radio sources the two effects affect the number-count almost equally.

This paper is organized as follows: in Section 2 we describe our method, and search for dipole anisotropy in the NVSS data alone (Section 3). Then we introduce the SUMSS catalogue (Section 4) and patch NVSS and SUMSS together (Section 5), exploring different ways of doing so. In Section 6 we perform a thorough clean up of local sources by cross-correlating NVSUMSS with the 2MRS catalogue. We investigate the effects of various cuts made on the inferred dipole velocity and discuss the statistical significance of the result (Section 7). We present our conclusions in Section 9.

2 THE METHOD

The aberration angle, $\Delta\theta$, by which a galaxy is displaced due to the motion of an observer moving with velocity v is (e.g. Kopeikin, Efroimsky & Kaplan 2011) for small velocities $v \ll c$:

$$\Delta\theta = (|v|/c)\sin\theta. \quad (1)$$

To evaluate this we simply count the number of galaxies in hemispheres and use the relation of the hemispherical number count asymmetry, δN, to the aberration angle:

$$\Delta\theta = 2(\delta N/N). \quad (2)$$

Here, we have assumed a homogeneous distribution with an average number surface density, and not taken into account any masks and cuts on the catalogue.

The total number asymmetry is due to both aberration and Doppler boosting. The expected amplitude of the latter is (Ellis & Baldwin 1984): $(v/c)[2 + x(1 + \alpha)]$, where x and α are flux indices, defined through the integral source counts

$$\mathrm{d}N/\mathrm{d}\Omega(>S) = kS^{-x}, \quad (3)$$

and the flux density at a fixed observing frequency

$$S_{\rm obs} = S_{\rm rest}\delta^{1+\alpha}. \quad (4)$$

It is straightforward to evaluate x for a given catalogue, e.g. as shown in Fig. 1 it varies from 0.894 at low flux to 1.68 at high flux for NVSS. The Doppler shift is more important for faint galaxies, hence the value at low flux is most relevant. The value of α is usually taken to be 0.75 (Ellis & Baldwin 1984). Hence, the aberration and Doppler boosting contribute almost equally to the number count asymmetry –53 per cent and 47 per cent respectively.

As we are looking specifically for a dipole anisotropy (to compare with the CMB dipole), we do not use spherical harmonic decomposition. The simplest and most robust estimate of the dipole is just the hemispheric asymmetry in the number count of sources. We calculate this as follows: first by randomly selecting a direction and counting the number of galaxies in that hemisphere. Secondly by regularly rotating a hemisphere centred on zero declination and looking for the right ascension that gives the maximum asymmetry. Third by scanning the sky using directions from a HEALPIX map (Gorski et al. 2005) with Nside = 32 (12 288 pixels) which are not random directions but regularly spaced. As we shall show, all these methods give similar results in agreement with each other. While the hemispheric asymmetry estimator is robust and allows the estimation of the variability of the dipole around its directional maximum, its statistical variability is high. Hence, we also evaluate the dipole using a three-dimensional linear estimator (Crawford 2009). Other estimators have been proposed in the literature (Chen & Schwarz 2016).

3 NRAO VLA SKY SURVEY (NVSS)

The NVSS is a catalogue of radio sources at 1.4 GHz which cover the sky north of declination -40° (the lowest source is actually at $-40\overset{\circ}{.}4$.) corresponding to 82 per cent of the celestial sphere (Condon 1989). It contains 1773 488 sources with flux density above 2.5 mJy. However, we restrict our analysis to sources brighter than 10 mJy as the completeness of the survey at weaker flux levels is questionable (Overzier et al. 2003). We also restrict the sources to be less bright than 1000 mJy as a relatively small number of very powerful sources can introduce large statistical fluctuations.

We further cut out the catalogue above Dec. = 40° in order to restore the symmetry necessary for extracting the dipole (Singal 2011). The catalogue is shown in the left panel of Fig. 1. The right panel shows how the integral number count changes with the threshold flux, which we use to determine the power-law index x in equation (3) finding it to be 0.894 and 1.68 at the low and high ends. We cut the Galactic plane by $\pm 5^\circ$, and then by $\pm 10^\circ$, and study the resulting catalogues adopting flux thresholds of 10,15, 20 and 25 mJy.

The results of our hemispheric asymmetry analysis are shown in Tables 2 and 3 and in Fig. 2. The results in the figure were obtained by cutting out the NVSS sources above Dec. = 40° to match the missing southern part below Dec. = -40°, and the Galactic plane was also cut at $\pm 10^\circ$. The dipole direction in all cases is close to that of the CMB dipole but its magnitude is on average about four times larger than that for the CMB (see Fig. 3).

4 SYDNEY UNIVERSITY MOLONGLO SKY SURVEY (SUMSS)

SUMSS is a radio imaging survey of the sky south of declination -30° carried out with the Molonglo Observatory Synthesis Telescope (MOST) operating at 843 MHz (Mauch et al. 2003). SUMSS contains 211 050 radio sources and is similar in sensitivity and resolution to the NVSS. The analysis of the catalogue shows that it is highly uniform and complete to 8 mJy at Dec. $\leq -50^\circ$, and to 18 mJy at $-30^\circ \geq$ Dec. $> -50^\circ$. An Aitoff plot is shown in Fig. 4.

For a robust dipole analysis a full-sky catalogue is required, so we combine NVSS and SUMSS. There are different ways of doing so which can potentially yield different results. This is discussed in the next section.

Table 2. Hemispheric asymmetry, NVSS (with the Northern cap removed at Dec. = 40° for symmetry with the missing Southern part, uses 5000 random hemispheres): Galactic latitude Cut (±), flux threshold (mJy), total number of sources left after cuts, average numbers in each hemisphere $\bar{N}$, maximum difference in number count of hemispheres ΔN, Dipole RA (deg), Dipole Dec. (deg), velocity (km s^{-1}).

b cut	Flux cut	N	$\bar{N}$	ΔN	RA°	Dec.°	v (km s^{-1})
5	10	416 389	208 180	4580	100.6	77.1	1657.5
5	15	299 409	149 704	3762	142.9	− 6.1	1899.2
5	20	233 277	116 631	3565	148.2	− 10.8	2294.9
5	25	189 995	95 012	3081	150.6	− 35.1	2438.8
10	10	384 844	192 391	4096	104.6	77.3	1644.8
10	15	276 524	138 281	3220	148.1	− 10.9	1732.6
10	20	215 418	107 725	3018	148.9	− 11.5	2119.2
10	25	175 383	87 713	2690	143.9	− 5.9	2296.4

Table 3. Hemispheric asymmetry, NVSS (with the Northern cap removed at Dec. = 40° for symmetry with missing Southern part, using HEALPIX grid of Nside = 32): super-Galactic latitude cut (±), Galactic latitude Cut (±), flux threshold (mJy), total number of sources left after cuts, Dipole Dec. (deg), Dipole RA (deg), Dipole value, Galactic b (deg), Galactic l (deg), velocity (km s^{-1}).

SGB cut	b cut	Flux cut	N	Dec.°	RA°	D	b°	l°	v (km s^{-1})
0	5	10	413 254	76.8	105.0	0.012	26.8	137.7	1502
0	5	15	297 806	− 17.0	150.5	0.013	29.7	255.0	1668
0	5	20	232 256	− 32.8	153.3	0.016	19.2	268.4	2054
0	5	25	189 357	− 32.8	153.3	0.017	19.2	268.4	2183
0	10	10	381 951	76.8	105.0	0.011	26.8	137.7	1447
0	10	15	275 168	− 15.7	149.1	0.012	29.7	252.9	1530
0	10	20	214 643	− 17.0	147.7	0.014	27.8	252.8	1859
0	10	25	174 881	− 6.0	143.4	0.015	31.9	240.1	1992
5	5	10	384 647	76.8	105.0	0.012	26.8	137.7	1619
5	5	15	277 131	− 17.0	150.5	0.013	29.7	255.0	1682
5	5	20	216 046	− 32.8	153.3	0.015	19.2	268.4	2002
5	5	25	176 136	− 32.8	153.3	0.016	19.2	268.4	2105
5	10	10	353 344	76.8	105.0	0.012	26.8	137.7	1569
5	10	15	254 493	− 15.7	149.1	0.012	29.7	252.9	1535
5	10	20	198 433	− 17.0	147.7	0.014	27.8	252.8	1785
5	10	25	161 660	− 6.0	143.4	0.015	31.9	240.1	1891
10	5	10	356 540	58.9	139.3	0.012	41.6	156.6	1532
10	5	15	256 877	− 17.0	150.5	0.013	29.7	255.0	1703
10	5	20	200 321	− 32.8	153.3	0.015	19.2	268.4	2000
10	5	25	163 267	− 32.8	153.3	0.016	19.2	268.4	2081
10	10	10	325 237	76.8	105.0	0.011	26.8	137.7	1432
10	10	15	234 239	− 15.7	149.1	0.012	29.7	252.9	1546
10	10	20	182 708	− 17.0	147.7	0.014	27.8	252.8	1765
10	10	25	148 791	− 6.0	143.4	0.014	31.9	240.1	1846

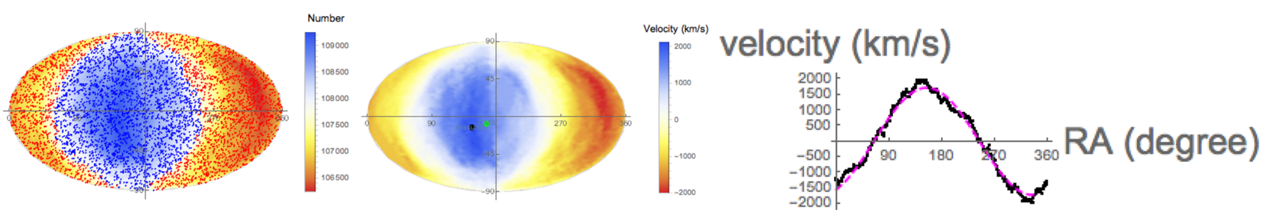

Figure 2. NVSS: The left panel shows the directions of 5000 randomly selected hemispheres which are used for number counts. The blue dots represent hemispheres with more-than-average number of galaxies, while red dots indicate those with less-than-average number of galaxies. The middle panel is a density plot of the magnitude of the velocity, upon which the directions of the CMB dipole (green circle) and the inferred direction for the radio sources (black circle) are marked. The right panel is the plot of the derived velocities (black dots) against the RA, which is fitted well by a cosine curve (magenta).

5 FULL SKY CATALOGUE: NVSS PATCHED WITH SUMSS (NVSUMSS)

We fill in the missing sky in NVSS by combining it with its southern counterpart SUMSS. To address overlapping regions, we generate the composite catalogue in two ways. In the first, SUMSS is cut at Dec. = −40° and joined to NVSS, while in the second NVSS is cut at Dec. = −30° and joined to SUMSS, as shown in Fig. 5. The right panel of Fig. 5 shows how the integral number count changes with

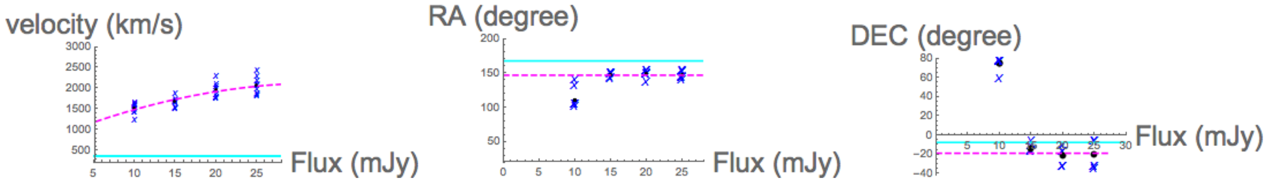

Figure 3. NVSS: The magnitude and direction of the velocity inferred from the radio dipole with various Galactic and super-Galactic cuts, and also with the LRS and the 2MRS sources removed and different patching schemes (black crosses). The black circles are the mean values at each flux and the dashed line is the fit to the mean, given by the quadratic $|v| = 823 + 86S - 1.34S^2$, where S is the flux threshold in mJy. Dashed (magenta) lines are the least-squares fits which give a mean velocity of 1918 ± 298 km s^{-1} in the direction RA $= 147^{\circ}$, Dec. $= -18\overset{\circ}{.}5$. The solid (cyan) line is the corresponding value inferred from CMB temperature dipole.

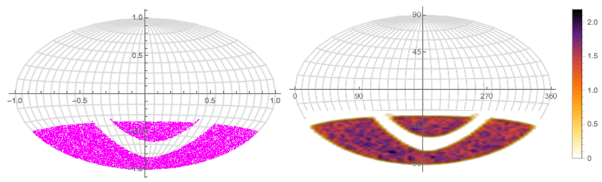

Figure 4. An Aitoff projection of the SUMSS catalogue (left) and its density plot (right).

the flux threshold which we use to determine the power x in equation (3). For NVSUMSS we find it to be 0.90 (cf. 0.894 for NVSS) and 1.7 (cf. 1.68 for NVSS) at the low and high ends. To correct for the frequency difference between the SUMSS and NVSS surveys, the SUMSS fluxes are scaled down by a factor of $(843/1400)^{-\alpha} \simeq 1.46$, where $\alpha \simeq 0.75$ is the median spectral index of the sources common to NVSS and SUMSS (Mauch et al. 2003).

Furthermore, NVSS and SUMSS have different source densities with SUMSS being denser. This can be dealt with in different ways. In the first, we randomly select galaxies from the SUMSS catalogue with declination below -40° (or below -30°) to match the same number as NVSS above Dec. $= 40^{\circ}$ (or 30°). In the second approach we evaluate the source density of NVSS in the full catalogue, and also that of SUMSS, and then pick randomly from SUMSS such that its density matches that of NVSS. Thirdly, when evaluating the three-dimensional linear estimator, we weight SUMSS sources by a factor corresponding to the ratio between the number of NVSS sources above Dec. $= 40^{\circ}$ (or 30°) and SUMSS sources below Dec. $= -40^{\circ}$ (or -30°). Although in the patching scheme we run the risk of smoothing out any dipole lying in the cap regions, as we shall show these different ways of producing the composite catalogue in fact yield rather similar results. The radio dipole still implies a large velocity in a direction close to that of the CMB dipole, as shown in Tables 4 and 5, and in Figs 6 and 7.

To ensure that the Galactic plane is not producing spurious effects on the inferred radio dipole, we also fill the Galactic plane with a random distribution of sources having the same surface density as the NVSUMSS catalogue. The results are presented in Table 6 and Fig. 7 shows that they do not change significantly.

6 DEALING WITH LOCAL ANISOTROPY

Any clustering of nearby sources can invalidate our approach, as both aberration and Doppler boosting analysis rely on the source distribution being isotropic so the only anisotropy is due to the observer's motion. Since the NVSS and SUMSS sources are mainly at redshift $z \sim 1$ (Ho et al. 2008; de Zotti et al. 2010) local anisotropies must be minimal, nevertheless we guard against them carefully as follows.

First we cross-correlate our composite NVSUMSS catalogue with the catalogue of nearby radio sources (van Velzen et al. 2012). However, the latter only contains bright radio-galaxies. In order to make sure that our composite catalogue is cleaned of *all* local sources, we go even further. We identify all local superclusters up to the Shapley concentration and remove them from NVSUMSS. Next, we remove the super-Galactic plane in which most dominant local structures lie. The final removal of all local sources is achieved by cross-correlating NVSUMSS with the 2MRS catalogue. We thus ensure as best as we can that *no* nearby sources are left in our composite catalogue.

6.1 Cross-correlation of NVSUMSS with LRS

The radio sources from the NVSS and SUMSS surveys have been matched to 2MRS galaxies using an image-level algorithm that properly treats the extended structure of radio sources (van Velzen et al. 2012). These bright sources constitute the all-sky LRS catalogue containing 575 radio-emitting galaxies with flux greater than

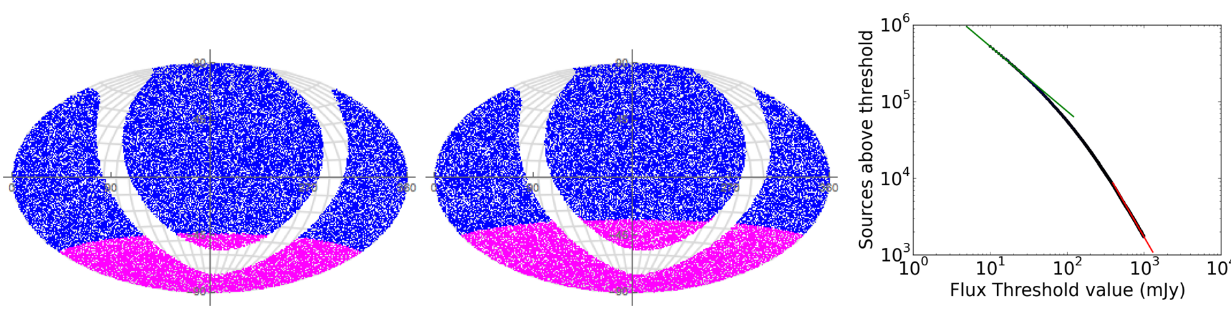

Figure 5. NVSUMSS: The left panel shows SUMSS cut at Dec. $= -40^{\circ}$ and joined with NVSS, while the middle panel shows NVSS cut at Dec. $= -30^{\circ}$ and joined with SUMSS. The right panel shows the integral number of sources in NVSUMSS above a flux threshold. Also shown is the fit of equation (3) at low and high flux which yields x of 0.9 and 1.7, respectively

Table 4. Hemispheric asymmetry, NVSUMSS (using 5000 random hemispheres): Galactic latitude cut (±), NVSS-SUMSS patch declination, flux threshold (mJy), total number of sources left after cuts, average numbers in each hemisphere $\bar{N}$, maximum difference in number counts of hemispheres ΔN, Dipole Dec. (deg), Dipole RA (deg), velocity (km s^{-1})

b cut	Patch cut	Flux cut	N	$\bar{N}$	ΔN	RA$^{\circ}$	Dec.$^{\circ}$	v (km s^{-1})
10	−40.	10	576 461	288 212	5880	151.3	−16.5	1570.9
10	−40.	15	413 838	206 932	5165	148.2	−13.1	1861.6
10	−40.	20	322 452	161 229	4422	148.0	−16.8	2056.1
10	−40.	25	262 617	131 297	3538	149.8	−12.9	1990.5
10	−30.	10	576 617	288 311	6468	148.8	−1.3	1673.0
10	−30.	15	413 564	206 768	5456	152.6	−17.4	1999.9
10	−30.	20	322 074	161 020	4304	151.3	−15.0	2017.6
10	−30.	25	262 332	131 149	3510	149.5	−13.3	2005.9

Table 5. Hemispheric asymmetry, NVSUMSS (using HEALPIX grid of Nside = 32): super-Galactic latitude cut (±), Galactic latitude Cut (±), NVSS-SUMSS patch declination, flux threshold (mJy), total number of sources left after cuts, Dipole Dec. (deg), Dipole RA (deg), Dipole value, Galactic b (deg), Galactic l (deg), velocity (km s^{-1})

SGB cut	b cut	Patch cut	Flux cut	N	Dec.$^{\circ}$	RA$^{\circ}$	D	b	l	v (km s^{-1})
0	10	−40	10	571 017	−13.2	149.1	0.0084	31.4	250.8	1094
0	10	−40	15	410 966	−13.2	149.1	0.0111	31.4	250.8	1436
0	10	−40	20	320 577	−17.0	150.5	0.0117	29.7	255.0	1520
0	10	−40	25	261 293	−17.0	150.5	0.0128	29.7	255.0	1656
0	10	−30	10	571 982	−13.2	149.1	0.0076	31.4	250.8	987
0	10	−30	15	411 258	−13.2	149.1	0.0109	31.4	250.8	1409
0	10	−30	20	320 651	−17.0	150.5	0.0118	29.7	255.0	1530
0	10	−30	25	261 363	−17.0	150.5	0.0113	29.7	255.0	1461
5	10	−40	10	517 269	−13.2	149.1	0.0090	31.4	250.8	1169
5	10	−40	15	372 124	−17.0	150.5	0.0113	29.7	255.0	1463
5	10	−40	20	290 194	−15.7	151.9	0.0116	31.5	255.1	1507
5	10	−40	25	236 448	−10.8	146.3	0.0124	31.0	246.5	1609
5	10	−30	10	518 021	−13.2	149.1	0.0088	31.4	250.8	1143
5	10	−30	15	372 370	−17.0	150.5	0.0108	29.7	255.0	1397
5	10	−30	20	290 249	−17.0	147.7	0.0111	27.8	252.8	1438
5	10	−30	25	236 574	−13.2	149.1	0.0115	31.4	250.8	1486
10	10	−40	10	464 161	−13.2	149.1	0.0100	31.4	250.8	1295
10	10	−40	15	334 073	−13.2	149.1	0.0129	31.4	250.8	1673
10	10	−40	20	260 580	−14.5	150.5	0.0118	31.5	253.0	1529
10	10	−40	25	212 239	−10.8	146.3	0.0120	31.0	246.5	1551
10	10	−30	10	464 926	−13.2	149.1	0.0098	31.4	250.8	1265
10	10	−30	15	334 335	−13.2	149.1	0.0127	31.4	250.8	1646
10	10	−30	20	260 539	−13.2	149.1	0.0118	31.4	250.8	1530
10	10	−30	25	212 219	−13.2	149.1	0.0116	31.4	250.8	1503

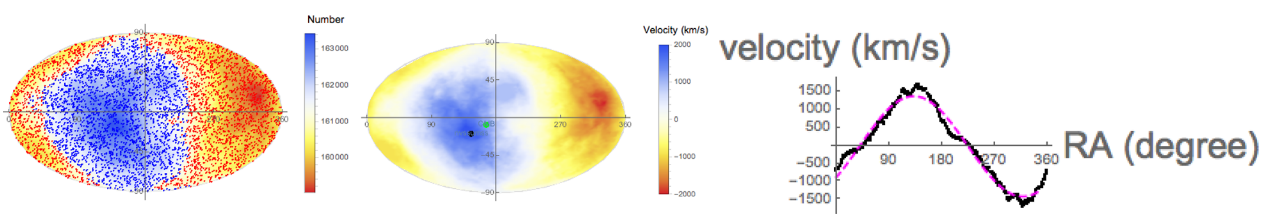

Figure 6. NVSUMSS catalogue (20–1000 mJy): The NVSS catalogue merged with SUMSS (cut at Dec. = −40°) and the Galactic plane cut at latitude of ±10° off NVSS to match the cut of SUMSS. The left panel shows number counts in 5000 randomly oriented hemispheres with an average of 288 218 galaxies per hemisphere and maximum difference of 5672 between the most and least populated hemispheres. The blue dots represent hemispheres which contain more-than-average number of galaxies, while red dots indicate those with less-than-average number of galaxies. The middle panel is a density plot of the magnitude of the inferred velocity, upon which the directions of the CMB dipole (green circle) and the inferred direction for the radio sources (black circle) are marked. The right panel is the plot of inferred velocities (black dots) against RA, which is well fitted by a cosine (magenta) curve.

213 mJy at 1.4 GHz. However, this means that nearby sources with flux less than 213 mJy are *not* identified and we shall address this in the following subsections. Here, we cross-correlate the LRS catalogue with our composite NVSUMSS catalogue and remove zones of increasingly larger area, starting at $1/10^{\circ}$ then $1/4^{\circ}$ then $1/2^{\circ}$, around the LRS sources. The results of the cross-correlation are presented in Table 7. The dipole of the LRS, using hemispherical number count, is shown in Fig. 8. This shows that the contribution

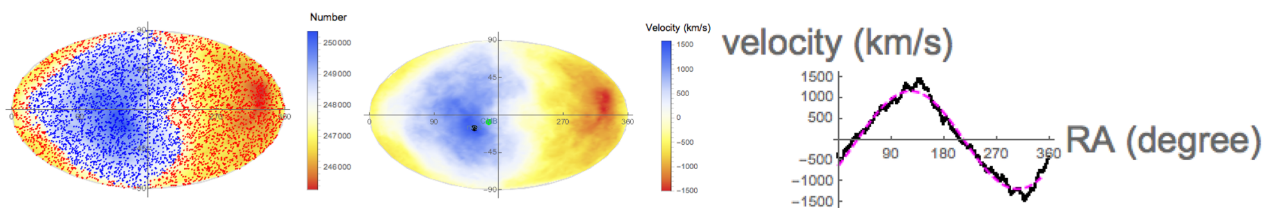

Figure 7. NVSUMSS with the Galactic plane filled with a random distribution having the same number density as the rest of the catalogue. The flux range is 15–1000 mJy and the details of the catalogues used in this figures are given in Table 6. The left panel shows the directions of hemispheres with blue corresponding to those having average count greater than mean and red to those with average count less than the mean. The middle panel is the magnitude of the velocity inferred from the number-count hemispherical asymmetry. The right panel is obtained by regularly rotating hemispheres in the RA direction at a 1° interval.

Table 6. Hemispheric asymmetry, NVSUMSS (with Galactic plane filled with a random distribution; uses 5000 random hemispheres): Galactic latitude cut (±), NVSS-SUMSS patch declination, flux threshold (mJy), total number of sources left after cuts, average numbers in each hemisphere $\bar{N}$, maximum difference in number counts of hemispheres ΔN, Dipole RA (deg), Dipole Dec. (deg), velocity (km s^{-1}).

b cut	Patch cut	Flux cut	N	$\bar{N}$	ΔN	RA°	Dec.°	v (km s^{-1})
10	−40	10	689 995	345 007	5743	149.0	−14.3	1306.3
10	−40	15	495 573	247 804	5164	149.2	−13.8	1590.6
10	−40	20	386 549	193 283	4428	150.0	−17.3	1722.6
10	−40	25	314 213	157 107	4200	148.8	−13.3	2003.6
10	−30	10	690 314	345 146	6954	159.0	−20.9	1512.8
10	−30	15	495 366	247 685	5432	152.3	−16.2	1647.3
10	−30	20	385 862	192 957	4371	152.3	−16.2	1711.2
10	−30	25	313 849	156 947	4193	149.6	−14.5	2006.9

Table 7. Hemispheric asymmetry, NVSUMSS (using 5000 random hemispheres): area in $degree^2$ around sources in LRS which is removed from NVSUMSS, Galactic latitude cut (±), NVSS-SUMSS patch declination, flux threshold (mJy), total number of sources left after cuts, average numbers in each hemisphere $\bar{N}$, maximum difference in number counts of hemispheres ΔN, Dipole RA (deg), Dipole Dec. (deg), velocity (km s^{-1}).

Area cut	b cut	Patch cut	Flux cut	N	$\bar{N}$	ΔN	RA°	Dec.°	v (km s^{-1})
$1/10^{\circ 2}$	10	−40	15	411 828	205 918	5275	150.2	−13.8	1922.4
$1/4^{\circ 2}$	10	−40	15	410 745	205 369	5072	150.6	−17.4	1842.4
$1/2^{\circ 2}$	10	−40	15	409 027	204 511	4745	152.5	−17.2	1768.7

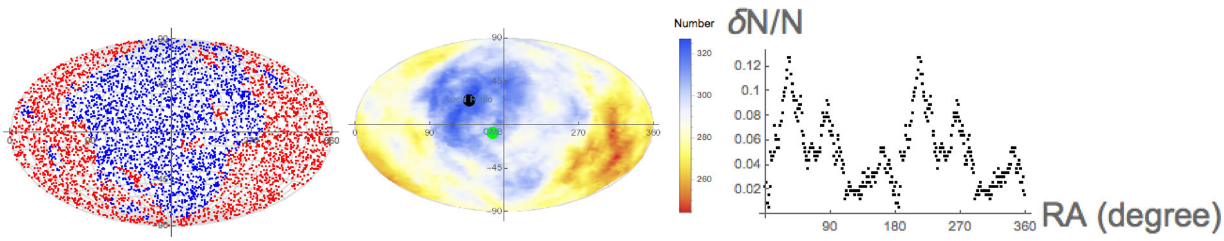

Figure 8. The left panel shows the directions of 5000 randomly placed hemispheres in the LRS catalogue of 575 radio galaxies in the local universe, with blue corresponding to those having average count greater than the mean (of 288) and red to those with average count less than the mean. The middle panel shows that a meaningful dipole cannot be seen in such a sparse and inhomogeneous sample. This is illustrated further in the right panel which plots the fractional number count difference between the forward and backward hemispheres versus the RA of the chosen direction.

of LRS sources to the large-scale dipole observed in NVSS and NVSUMSS is insignificant.

6.2 Elimination of large superclusters up to Shapley and Ophiuchus

The origin of the CMB dipole is supposedly due to the gravitational attraction of nearby inhomogeneities. A large part of it can indeed be attributed to local superclusters (Lavaux et al. 2010; Colin et al. 2011). These superclusters are well observed and their position is indicated in Table 1. [We note that in a previous study (Blake & Wall 2002) 22 local sources were removed; however it is not clear what these sources were.] The results presented in Table 8 show that the dipole velocity is not affected by these eliminations.

6.3 Removing the super-Galactic plane

The most important superclusters in our local Universe define the super-Galactic plane which may contain a significant number of radio sources (Shaver & Pierre 1989). Hence, one way of removing

Table 8. Hemispheric asymmetry, NVSUMSS (using 5000 random hemispheres): area in degree[2] around the 8 local superclusters (see Table 1), Galactic latitude cut (±), NVSS-SUMSS patch declination, flux threshold (mJy), total number of sources left after cuts, average numbers in each hemisphere $\bar{N}$, maximum difference in number counts of hemispheres ΔN, Dipole RA (deg), Dipole Dec. (deg), velocity (km s^{-1}). In total about 5000 to 6000 sources are removed.

Area cut	b cut	Patch cut	Flux cut	N	$\bar{N}$	ΔN	RA°	Dec.°	v (km s^{-1})
$1/10^{\circ 2}$	10	−40	15	409 025	204 477	4709	151.4	−16.5	1788.5
$1/4^{\circ 2}$	10	−40	15	409 011	204 488	4885	151.4	−16.4	1805.5
$1/2^{\circ 2}$	10	−40	15	408 989	204 492	4683	146.8	−12.8	1703.6

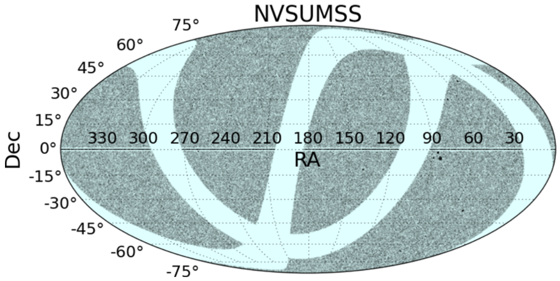

Figure 9. NVSUMSS with Galactic and super-Galactic planes removed as strips of ±10° each.

local sources is to remove this plane. Fig. 9 shows the NVSUMSS map with both the Galactic and super-Galactic planes cut out as ±10° strips. However, this makes little difference to either the magnitude or the direction of the radio dipole as seen from the results in Tables 9 and 10.

6.4 Cross-correlation of NVSUMSS with 2MRS

There may still be local sources not lying on the super-Galactic plane, or not included in our list of prominent superclusters, or with flux less than 213 mJy. In order to be certain that *all* local sources have indeed been removed, we cross-correlate NVSUMSS with the 2MRS catalogue (Huchra et al. 2012) and remove all common objects. This is done by identifying all NVSUMMS sources that are within a chosen angular distance of 2MRS sources – we try various values: 1, 10 and 36 arcsec. The full set of results is shown in Figs 10 and 11 and all details are also given in Tables 9 and 10. These demonstrate that the inferred velocity from the radio dipole remains well above that from the CMB dipole, although the directions are close.

7 STATISTICAL SIGNIFICANCE

To determine the statistical significance of our results, we compare them with Monte Carlo simulations using randomly generated isotropic catalogues, on top of which aberration and Doppler boosting dipoles are added according to the null hypothesis that we are travelling through the CMB with a velocity of 369 km s^{-1} towards $l = 263.85°$, $b = 48.25°$. A sample of size N is expected to contain random hemispherical asymmetries of size $\sim 1/\sqrt{N}$ on average, the direction of the dipole being random. An aberration effect corresponding to what is expected from our velocity of 369 km s^{-1} with respect to the CMB is subsequently applied to these catalogues by shifting the angles in the direction of the CMB dipole by the expected amount. A dipole due to Doppler boosting can also be incorporated by adding (subtracting) the appropriate number of sources within angular rings oriented in (opposite to) the direction of the CMB dipole. The hemispheric asymmetry and three-dimensional linear estimators can subsequently be applied to the resultant random catalogues to extract the velocity.

In 2000 mock catalogues with about 600 000 sources generated as above, the hemispheric count estimator observed velocities larger than the inferred 1600 km s^{-1} for 741 of these. The inferred dipole direction was within 15° of the (simulated) CMB dipole direction for 690 of these. For the same 2000 catalogues, the three-dimensional linear estimator found velocities higher than the inferred 1300 km s^{-1} for only five of the catalogues, all of which had dipole directions within 10° of the (simulated) CMB dipole direction. Consequently, the statistical significance of the latter observation is at the level of $p \simeq 0.0025$, i.e. 2.81σ (99.75 per cent confidence).

8 THE BIAS

It has been noted previously that the three-dimensional estimator that we have used here is biased (Rubart & Schwarz 2013). Using Monte Carlo simulations we therefore evaluate:

$$\text{Bias factor} \approx \frac{|\text{True dipole} + \text{Random Dipole}|}{|\text{True dipole}|} \quad (5)$$

for both our estimators, where 'true' refers to the CMB dipole. The bias depends on whether and by how much the Galactic plane and the super-Galactic plane are cut. We consider just two cases: the Galactic plane cut of ±10°, and the Galactic as well as the super-Galactic plane cut of ±10°. The results are shown in Fig. 12. As expected the bias decreases as the sample size increases. The bias factor explicitly depends on the *true* velocity which we have assumed to be 369 km s^{-1}. The bias factor for the hemispheric number-count estimator, at the catalogue size of ∼500 000–600 000 relevant to NVSUMSS, is about 1.9, while for the three-dimensional estimator it is about 1.3. This explains why the inferred velocity with the former estimator is about 1600 km s^{-1} while for the latter estimator it is about 1200 km s^{-1}. The agreement between them improves when the velocities are scaled down by the corresponding bias factors.

The bias does *not* affect the statistical significances of our results as presented in the previous section, since it applies *equally* to both the observational data and the null trials.

9 CONCLUSION

The velocity of the barycentre of our Solar system (or of the Local Group) in the rest frame of CMB is inferred from its temperature dipole anisotropy. An independent measurement of this velocity is needed to fully establish the kinematical origin of the dipole. Although a similar anisotropy is observed in the distribution of nearby large-scale structure out to the Shapley supercluster, they do *not* show full convergence to the CMB dipole. To definitively address this question one thus needs to go further; however there are no data available from optical or infrared galaxy surveys.

Table 9. Hemispheric asymmetry, NVSUMSS cross-correlated with 2MRS to remove local sources (using HEALPIX grid of Nside = 32). Only a sample of results is shown (full table is available in the online version of the article). (1) Angular tolerance within which 2MRS sources are looked for, (2) number of sources removed because of 2MRS overlap, (3) super-Galactic latitude cut (±), (4) Galactic latitude cut (±), (5) NVSS-SUMSS patch declination, (6) flux threshold (mJy), (7) total number of sources left after cuts, (8) Dipole Dec. (deg), (9) Dipole RA (deg), (10) Dipole value, (11) Galactic b (deg), (12) Galactic l (deg), (13) velocity (km s^{-1}).

(1)	(2)	(3)	(4)	(5)	(6)	(7)	(8)	(9)	(10)	(11)	(12)	(13)
10 arcsec	3701	10	10	−40	10	460 484	−13.2	149.1	0.009	31.4	250.8	1368
10 arcsec	2510	10	10	−40	15	331 552	−13.2	149.1	0.011	31.4	250.8	1792
10 arcsec	1847	10	10	−40	20	258 813	−13.2	149.1	0.012	31.4	250.8	1873
10 arcsec	1470	10	10	−40	25	210 756	−13.2	149.1	0.011	31.4	250.8	1742
10 arcsec	1228	10	10	−40	30	177 191	−13.2	149.1	0.012	31.4	250.8	1898
10 arcsec	1036	10	10	−40	35	152 561	−10.8	146.3	0.012	31.0	246.5	1809
10 arcsec	897	10	10	−40	40	133 018	−10.8	146.3	0.011	31.0	246.5	1784
10 arcsec	788	10	10	−40	45	117 685	−13.2	149.1	0.012	31.4	250.8	1811
10 arcsec	710	10	10	−40	50	105 184	−52.8	174.6	0.013	8.5	291.9	2025
10 arcsec	3662	10	10	−30	10	461 202	−13.2	149.1	0.009	31.4	250.8	1484
10 arcsec	2499	10	10	−30	15	331 651	−13.2	149.1	0.010	31.4	250.8	1629
10 arcsec	1846	10	10	−30	20	258 767	−13.2	149.1	0.011	31.4	250.8	1740
10 arcsec	1456	10	10	−30	25	210 719	−12.0	144.8	0.011	29.2	246.6	1679
10 arcsec	1209	10	10	−30	30	177 340	−13.2	149.1	0.011	31.4	250.8	1749
10 arcsec	1016	10	10	−30	35	152 334	−10.8	146.3	0.010	31.0	246.5	1597
10 arcsec	877	10	10	−30	40	133 015	−10.8	146.3	0.011	31.0	246.5	1795
10 arcsec	776	10	10	−30	45	117 626	−13.2	149.1	0.012	31.4	250.8	1906
10 arcsec	699	10	10	−30	50	105 089	−52.8	174.6	0.012	8.5	291.9	1829

Table 10. Three-dimensional linear estimator, NVSUMSS, cross-correlated with 2MRS to remove local sources. Only a sample of results is shown (full table is available in the online version of the article.). (1) Angular tolerance within which 2MRS sources are looked for, (2) number of sources removed because of 2MRS overlap, (3) super-Galactic latitude cut (±), (4) Galactic latitude cut (±), (5) NVSS-SUMSS patch declination, (6) flux threshold (mJy), (7) total number of sources left after cuts, (8) Dipole Dec. (deg), (9) Dipole RA (deg), (10) Dipole value, (11) Galactic b (deg), (12) Galactic l (deg), (13) velocity (km s^{-1}).

(1)	(2)	(3)	(4)	(5)	(6)	(7)	(8)	(9)	(10)	(11)	(12)	(13)
10 arcsec	3654	10	10	−40	10	457 184	14.1	128.4	2468	28.9	211.2	1265
10 arcsec	2465	10	10	−40	15	329 034	5.9	128.2	1755	25.2	219.4	1250
10 arcsec	1807	10	10	−40	20	256 430	− 1.7	126.3	1453	19.9	225.7	1328
10 arcsec	1423	10	10	−40	25	208 861	− 4.3	127.6	1156	19.7	228.8	1297
10 arcsec	1196	10	10	−40	30	175 595	− 4.4	134.3	1058	25.4	232.7	1412
10 arcsec	1006	10	10	−40	35	150 883	− 11.5	136.8	840	23.3	240.7	1304
10 arcsec	870	10	10	−40	40	131 662	− 15.6	129.6	859	15.3	239.8	1529
10 arcsec	767	10	10	−40	45	116 504	− 15.3	143.0	751	25.7	248.0	1512
10 arcsec	693	10	10	−40	50	104 075	− 23.1	156.3	667	28.6	264.3	1502
10 arcsec	3602	10	10	−30	10	455 766	1.0	126.2	2417	21.1	223.2	1243
10 arcsec	2424	10	10	−30	15	327 749	− 0.4	125.8	1753	20.1	224.3	1253
10 arcsec	1769	10	10	−30	20	255 327	− 4.9	123.9	1394	16.2	227.4	1280
10 arcsec	1392	10	10	−30	25	208 009	− 8.5	122.9	1078	13.5	230.0	1215
10 arcsec	1171	10	10	−30	30	174 886	− 6.0	130.3	1003	21.1	231.8	1344
10 arcsec	989	10	10	−30	35	150 122	− 9.8	133.0	782	21.3	236.7	1221
10 arcsec	858	10	10	−30	40	131 043	− 12.1	128.2	839	16.1	236.1	1501
10 arcsec	753	10	10	−30	45	115 919	− 12.5	139.6	712	24.9	243.4	1440
10 arcsec	677	10	10	−30	50	103 530	− 17.0	152.8	625	31.2	256.9	1415

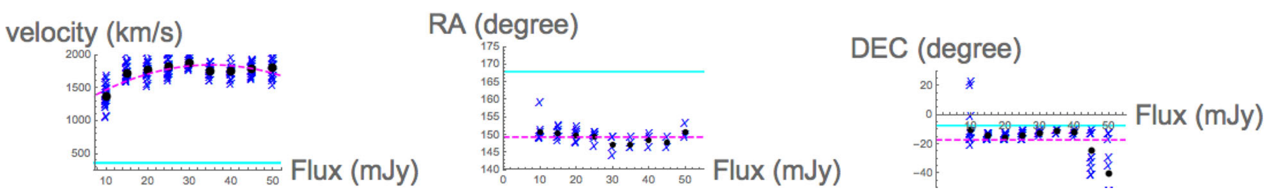

Figure 10. All results from NVSUMSS using the hemispherical number count estimator, with the Galactic and super-Galactic plane cut out and with LRS as well as 2MRS sources removed, and using different patching schemes (blue crosses). The black filled circles are the means for each flux and the dashed line is the least-squares fit to the data which yields the velocity $|v| = 1121 + 41S - 0.6S^2$, where S is the flux threshold in mJy. The cyan line is the value inferred from CMB temperature dipole.

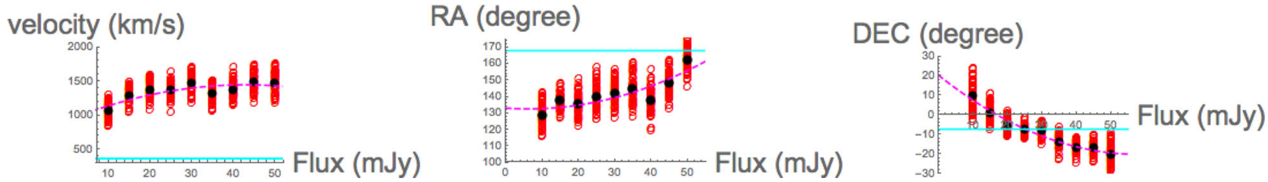

Figure 11. All results from NVSUMSS using the linear three-dimensional estimator, with the Galactic and super-Galactic plane cut out and with LRS as well as 2MRS sources removed, and using different patching schemes (red circles). The black filled-circles are the means for each flux threshold used and the dashed line is the least-squares fit to the data which yields the velocity $|v| = 926.7 + 24.4S - 0.28S^2$, where S is the flux threshold in mJy. The cyan line is the value inferred from CMB temperature dipole.

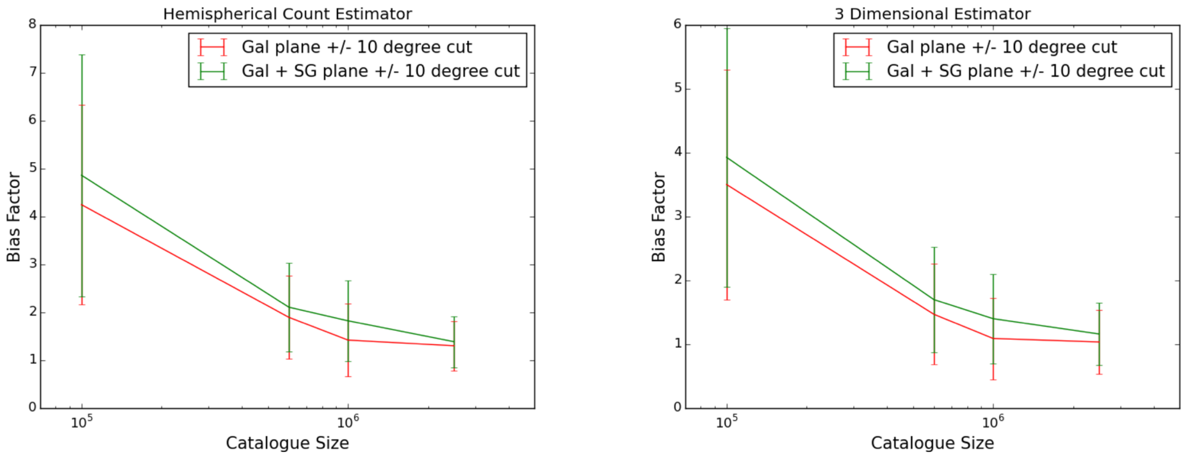

Figure 12. Bias factor versus catalogue size for the hemispheric number-counts (left) and for the three-dimensional estimator (right).

Radio surveys which sample the Universe at high redshift provide valuable clues to this problem. As these scales are certainly large enough for the Universe to be considered homogeneous and isotropic (aside from negligible statistical fluctuations), the only source of deviation from isotropy would be due to the motion of the observer. Our motion should lead to a measurable overdensity of sources in the direction of motion through aberration and Doppler boosting effects. By measuring these effects we can deduce our velocity in the rest frame of the radio galaxies, its expected value being just our velocity in the CMB rest frame. NVSS is a radio catalogue with less-than-complete sky coverage which has been used extensively to extract this velocity but previous studies have generally found its value to be far larger than our velocity in the CMB rest frame. We confirm this surprising result using an all-sky catalogue.

A possible reason for this discrepancy could be bias due to local structures. Of course, one does not expect such anisotropies to produce a dipole *larger* than the CMB dipole. However, we know that our local Universe at least up to 260 Mpc ($z \simeq 0.06$) is anisotropic and if our radio catalogue is contaminated by local sources, that may invalidate the method based on the aberration and Doppler boosting effects which rely on large-scale intrinsic isotropy. We adopt various measures to remove such local sources but find that this has little effect on the inferred radio dipole.

There is a big gap in redshift between local galaxies and the radio galaxies. Forthcoming galaxy surveys will progressively fill in this gap and hopefully allow us to trace the divergence from the CMB dipole. Future radio surveys with the Square Kilometre Array will provide excellent opportunities for improving the statistical significance of the unexpectedly large radio dipole (Schwarz et al. 2015).

ACKNOWLEDGEMENTS

JC and RM acknowledge support from the Nordea Foundation and hospitality at the Niels Bohr International Academy. This work was supported by a DNRF Niels Bohr Professorship awarded to SS. We thank Pavel Naselsky, Andy Jackson, Dominik Schwarz and Sjoert van Velzen for helpful discussions, and, especially, Prabhakar Tiwari for emphasizing the need for flux rescaling in assembling the NVSUMMS flux-limited catalogue and the anonymous referee who pointed out the need to estimate the bias in the estimators used.

REFERENCES

Atrio-Barandela F., Kashlinsky A., Ebeling H., Fixsen D. J., Kocevski D., 2015, ApJ, 810, 143
Baleisis A., Lahav O., Loan A. J., Wall J. V., 1998, MNRAS, 297, 545
Blake C., Wall J., 2002, Nature, 416, 150
Bracewell R. N., Conklin E. K., 1968, Nature, 219, 1343
Burles S., Rappaport S., 2006, ApJ, 641, L1
Challinor A., van Leeuwen F., 2002, Phys. Rev. D., 65, 103001
Chen S., Schwarz D. J., 2016, A&A, 591, A135
Chluba J., Hütsi G., Sunyaev R. A., 2005, A&A, 434, 811
Colin J., Mohayaee R., Sarkar S., Shafieloo A., 2011, MNRAS, 414, 264
Condon J. J., 1989, ApJ, 338, 13
Crawford F., 2009, ApJ, 692, 887
de Zotti G., Massardi M., Negrello M., Wall J., 2010, A&AR, 18, 1
Ellis G. F. R., Baldwin J. E., 1984, MNRAS, 206, 377
Feindt U. et al., 2013, A&A, 560, A90
Feldman H. A., Watkins R., Hudson M. J., 2010, MNRAS, 407, 2328
Ghosh S., 2014, Phys. Rev. D., 89, 063518
Gibelyou C., Huterer D., 2012, MNRAS, 427, 1994

Gorski K. M., Hivon E., Banday A. J., Wandelt B. D., Hansen F. K., Reinecke M., Bartelmann M., 2005, ApJ, 622, 759
Henry P. S., 1971, Nature, 231, 516
Ho S., Hirata C., Padmanabhan N., Seljak U., Bahcall N., 2008, Phys. Rev. D., 78, 043519
Huchra J. P. et al., 2012, ApJS, 199, 26
Hudson M. J., Smith R. J., Lucey J. R., Branchini E., 2004, MNRAS, 352, 61
Itoh Y., Yahata K., Takada M., 2010, Phys. Rev. D., 82, 043530
Kashlinsky A., Atrio-Barandela F., Kocevski D., 2008, ApJ, 686, L49
Kogut A. et al., 1993, ApJ, 419, 1
Kopeikin S., Efroimsky M., Kaplan G., 2011, Relativistic Celestial Mechanics of the Solar system. Wiley, Hoboken NJ
Langlois D., Piran T., 1996, Phys. Rev. D., 53, 2908
Lauer T. R., Postman M., 1994, ApJ, 425, 418
Lavaux G., Tully R. B., Mohayaee R., Colombi S., 2010, ApJ, 709, 483
Magoulas C., Springob C., Colless M., Jones D. H., Campbell L., Lucey J., Mould J., 2012, AAO Observer No. 122, p.10 (arXiv:1210.0625)
Mauch T., Murphy T., Buttery H. J., Curran J., Hunstead R. W., Piestrzynski B., Robertson J. G., Sadler E. M., 2003, MNRAS, 342, 1117
Overzier R. A., Röttgering H. J. A., Rengelink R. B., Wilman R. J., 2003, A&A, 405, 53
Paczynski B., Piran T., 1990, ApJ, 364, 341
Peebles P. J. E., Wilkinson David T., 1968, Phys. Rev. D., 174, 2168
Planck Collaboration XXVII, 2014, A&A, 571, A27
Plionis M., Coles P., Catelan P., 1993, MNRAS, 262, 465
Rubart M., Schwarz D. J., 2013, A&A, 555, A117
Schwarz D. J. et al., 2015, Proc. Sci., Testing Foundations of Modern Cosmology with SKA all-sky Surveys. SISSA, Trieste, PoS(AASKA14)032
Shaver P. A., Pierre M., 1989, A&A, 220, 35
Singal A. K., 2011, ApJ, 742, L23
Smoot G. F., Gorenstein M. V., Muller R. A., 1977, Phys. Rev. Lett., 39, 898
Stewart J. M., Sciama D. W., 1967, Nature, 216, 748
Tiwari P., Jain P., 2015, MNRAS, 447, 2658
Tiwari P., Nusser A., 2016, J. Cosmol. Astropart. Phys., 3, 062
Tiwari P., Kothari R., Naskar A., Nadkarni-Ghosh S., Jain P., 2015, Astropart. Phys., 61, 1
van Velzen S., Falcke H., Schellart P., Nierstenhöfer N., Kampert K.-H., 2012, A&A, 544, A18
Watkins R., Feldman H. A., 2015, MNRAS, 447, 132
Watkins R., Feldman H. A., Hudson M. J., 2009, MNRAS, 392, 743

SUPPORTING INFORMATION

Supplementary data are available at *MNRAS* online.

Table 9. Hemispheric asymmetry, NVSUMSS cross-correlated with 2MRS to remove local sources (using HEALPIX grid of Nside = 32).
Table 10. Three-dimensional linear estimator, NVSUMSS cross-correlated with 2MRS to remove local sources.

Please note: Oxford University Press is not responsible for the content or functionality of any supporting materials supplied by the authors. Any queries (other than missing material) should be directed to the corresponding author for the article.

This paper has been typeset from a TEX/LATEX file prepared by the author.